Materials Science & Engineering A 673 (2016) 378–390

Contents lists available at ScienceDirect

Materials Science & Engineering A

journal homepage: www.elsevier.com/locate/msea

Effects of Cr and Zr additions on microstructure and properties of Cu-Ni-Si alloys

Wei Wang [a], Huijun Kang [a], Zongning Chen [a], Zhongjun Chen [b], Cunlei Zou [a], Rengeng Li [a], Guomao Yin [a], Tongmin Wang [a,*]

[a] Key Laboratory of Solidification Control and Digital Preparation Technology (Liaoning Province), School of Materials Science and Engineering, Dalian University of Technology, Dalian 116024, PR China

[b] Beijing Synchrotron Radiation Facility, Institute of High Energy Physics and University of the Chinese Academy of Sciences, Chinese Academy of Sciences, Beijing 100043, PR China

ARTICLE INFO

Article history:
Received 3 May 2016
Received in revised form
17 June 2016
Accepted 7 July 2016
Available online 9 July 2016

Keywords:
Cu-Ni-Si alloy
High strength
High electrical conductivity
Ageing
Precipitation kinetics

ABSTRACT

Cu-Ni-Si alloys are widely used for electrical applications owing to high strength and high electrical conductivity. In this work, the effects of Cr and Zr additions on microstructure and properties of Cu-Ni-Si alloys were investigated. The addition of Cr and Zr results in formation of Cr_3Si and Ni_2SiZr intermetallic compounds, respectively, thus increases the electrical conductivity of Cu-Ni-Si alloy and refines the microstructure. Microstructure analysis confirms the presence of δ-Ni_2Si precipitates, which strengthens the alloy through Orowan mechanism. Alloying with Zr element deteriorates the mechanical property of Cu-Ni-Si alloy, whereas in the presence of Cr, to the contrary, the ultimate tensile strength is increased, whether Zr is incorporated or not. Moreover, the addition of Zr can decrease the stacking fault energy (SFE) and promote formation of deformation twins. The best integrated performance is obtained through co-addition of Cr and Zr elements. The ultimate strength, elongation and electrical conductivity are 706 MPa, 9.5% and 48.2% IACS, respectively. The precipitation kinetics was discussed in terms of Avrami equation and the activation energy of Ni_2Si precipitation was obtained. The calculated activation energies of precipitation are 105, 89, 115 and 111 kJ/mol for Cu-Ni-Si, Cu-Ni-Si-Zr, Cu-Ni-Si-Cr and Cu-Ni-Si-Cr-Zr alloy, respectively.

1. Introduction

Copper alloys exhibiting both high strength and high electrical conductivity are widely used for electrical applications, such as lead frames, railway contact wires and connectors [1–3]. Various copper alloys have been developed to meet industrial demands, such as Cu-Be [4], Cu-Cr [5–7], Cu-Fe-P [8], Cu-Ni-Si [9–11] and Cu-Mg [12] alloys. Of all the copper based alloy systems, precipitation strengthened Cu-Ni-Si system alloys have attracted much attention due to their ultrahigh strength and high electrical conductivity. The formation of Ni-Si precipitates in copper matrix increases the strength with minimum decrease in electrical conductivity [13]. Despite applications in electrical industry, the Cu-Ni-Si system alloys are also used as resistance welding electrodes and molding tolls, and are the preferred candidate material for the first wall of nuclear reactor [14,15].

In recent decades, attempts have been made to further improve the strength of Cu-Ni-Si alloys and addition of trace amount of alloying elements appears to be an effective way. Addition of Co element can form orthorhombic $(Ni, Co)_2Si$ precipitates sharing the same crystal system with Ni_2Si precipitates and decrease the inner-precipitate spacing as well as dislocation density [16,17]. Trace amount of P can suppress the discontinuous precipitation reaction, resulting in enhancement of both strength and elongation [18]. Adding Cr to a Cu-Ni-Si-P alloy decreases the grain size greatly [18]. V addition suppresses the recrystallization, retards the grain growth, and accelerates the precipitation of Ni_2Si metallic compounds [19]. The addition of trace Ti reduces grain size and greatly increases elongation. In addition, the equilibrium concentration of Ni_2Si in copper matrix is reduced and precipitation is accelerated by trace Ti [20].

Due to the low solubility of Cr and Zr in copper, Cu-Cr and Cu-Zr alloys are capable of preserving high electric conductivity [7,21]. Some of recent reports pointed out that Zr lowers the stacking fault energy in copper and thus contributes to higher work hardening [22,23]. In this study, trace amount of Cr and Zr additions were added to a Cu-2.0 wt%Ni-0.5 wt%Si alloy for the sake of

* Corresponding author.
E-mail address: tmwang@dlut.edu.cn (T. Wang).

http://dx.doi.org/10.1016/j.msea.2016.07.021
0921-5093/

Table 1
Designed and tested chemical compositions of Cu-Ni-Si alloys with Cr and Zr additions.

Alloys	Designed					Tested				
	Ni	Si	Cr	Zr	Cu	Ni	Si	Cr	Zr	Cu
CuNiSi	2	0.5	–	–	Bal.	1.9168	0.5226	/	/	Bal.
CuNiSiZr	2	0.5	–	0.15	Bal.	1.8670	0.4726	/	0.1608	Bal.
CuNiSiCr	2	0.5	0.3	–	Bal.	1.8275	0.4881	0.3957	/	Bal.
CuNiSiCrZr	2	0.5	0.15	0.15	Bal.	1.8794	0.5995	0.2158	0.2482	Bal.

improving mechanical property while maintaining electrical conductivity.

2. Experimental

Ingots of Cu-2.0 wt%Ni-0.5 wt%Si alloys with Cr and Zr additions were prepared by induction melting in a graphite furnace under argon atmosphere. The designed and tested chemical compositions are listed in Table 1. The ingots were casted at 1523 K in a quasi-cubic iron mold, homogenized at 1233 K for 24 h and hot-rolled with 66% reduction in thickness at 1123 K. The hot rolled sheets were solution treated at 1233 K for 1 h and quenched in water before cold rolled with 60% reduction at room temperature. These rolled plates were then isochronally aged for 1 h at various temperatures and isothermally aged at 723 K and 773 K for various time. As for tensile test, the rolled plates were pre-aged at 723 K for 1 h, cold rolled with 50% reduction and finally aged at 648 K for 8 h.

Microhardness tests were performed using Vickers method on a MH-50 type microhardness tester. The indentations were made with a diamond square-based pyramid under a load of 0.2 kg for 10 s dwelling time on well polished surface of samples. The test was repeated 5 times for each sample to obtain an arithmetic average value. For the electrical conductivity, a D60K digital electrical instrument was applied at 293 K and the results are presented by International annealed copper standard (IACS). The microstructures were observed using a JSM-5600LV type of scanning electronic microscopy (SEM) and an Olympus GX51 type of optical microscopy (OM). The samples were prepared by conventional mechanical polishing method and etched in an aqueous solution containing 3 g $FeCl_3$+95 ml C_2H_5OH+2 ml HCl. Transmission electron microscope (TEM) samples were obtained by double jet electrolytic-polishing at −30 °C within a bath containing 30% nitric acid and 70% methanol. The resulting foil specimens were observed under Talos F200 × microscope with an acceleration voltage of 200 kV. The synchrotron X-ray radiation analysis was performed at 4B9A beamline of Beijing Synchrotron Radiation Facility (BSRF). The samples were illuminated with a monochromatic X-ray beam at an energy of 8050 eV (λ=1.54 nm) to acquire an accurate measurement.

3. Results and discussions

3.1. Microstructure

3.1.1. Microstructure changes during thermomechanical treatment

Fig. 1 shows the optical macrostructures of as cast designed Cu-Ni-Si-(Cr-Zr) alloys. Large grains whose size exceeds several micrometers are observed in all cases owing to the low cooling speed of iron mold surrounded by sands. For raw Cu-Ni-Si alloys, typical

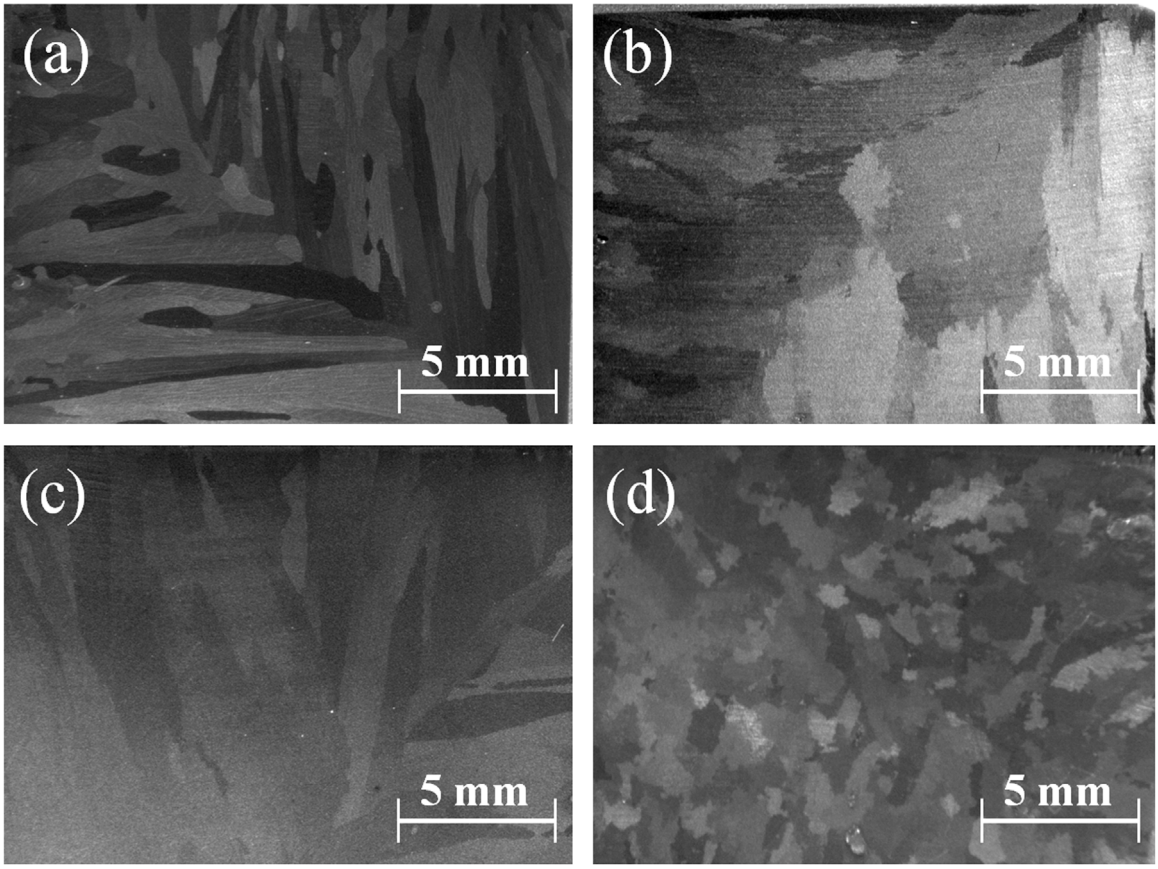

Fig. 1. Optical macrostructures of as cast Cu-Ni-Si alloys: (a) Cu-Ni-Si alloy; (b) Cu-Ni-Si-Zr alloy; (c) Cu-Ni-Si-Cr alloy; (d) Cu-Ni-Si-Cr-Zr alloy.

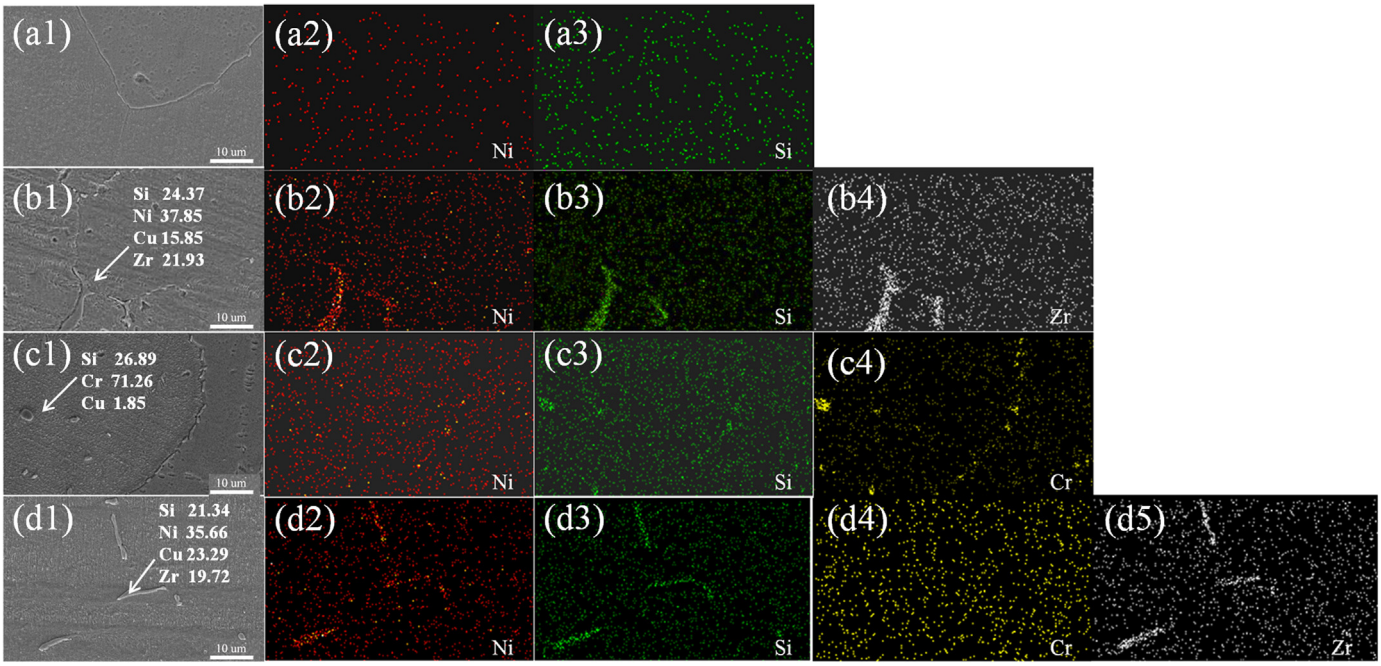

Fig. 2. SEM micrographs and the elemental mapping images of designed Cu-Ni-Si-(Cr-Zr) alloys after homogenization at 1233 K for 24 h: (a1)–(a3) Cu-Ni-Si alloy; (b1)–(b4) Cu-Ni-Si-Zr alloy; (c1)–(c4) Cu-Ni-Si-Cr alloy; (d1)–(d5) Cu-Ni-Si-Cr-Zr alloy.

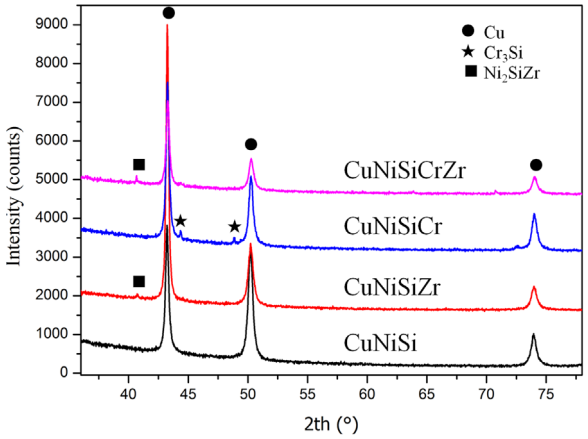

Fig. 3. Synchrotron X-ray diffraction patterns of designed Cu-Ni-Si-(Cr-Zr) alloys after homogenization at 1233 K for 24 h.

columnar grains prevail in the microstructure (Fig. 1(a)). The addition of Cr and Zr separately refines the grain size slightly while maintaining the columnar structure (Fig. 1(b) and (c)). However, the grains are significantly refined upon co-addition of Cr and Zr (Fig. 1(d)), and the morphology changes from columnar to quasi-equiaxed grains.

Fig. 2 shows the element distribution of designed Cu-Ni-Si-(Cr-Zr) alloys after homogenization at 1233 K for 24 h. For raw Cu-Ni-Si alloy, Ni and Si elements distribute uniformly in copper matrix and no intermetallic is observed. With the addition of Cr and Zr elements, intermetallic particles are observed. Elemental mapping images indicate that intermetallic particles are rich in Cr and Si for Cu-Ni-Si-Cr alloy and rich in Ni, Si, Zr for Cu-Ni-Si-Zr and Cu-Ni-Si-Cr-Zr alloys. According to Energy Dispersive Spectrometer (EDS) analysis, the compositions of the intermetallic particles are close to Ni_2SiZr, Cr_3Si and Ni_2SiZr respectively. Unlike Cu-Ni-Si-Cr alloy, Cr element distributes uniformly in Cu-Ni-Si-Cr-Zr alloy rather than segregates with Si element. Fig. 3 illustrates synchrotron X-ray diffraction patterns of designed alloys after homogenization at 1233 K for 24 h. Typical peaks of Cu can be identified in all cases and additional peaks are observed with Cr and Zr additions. Cr_3Si phase is indexed with Cr additions, and additional peak with Zr addition is attributed to the formation of Ni_2SiZr phase [24].

Fig. 4 illustrates the optical microstructure of solution treated alloys. Recrystallization took place and grains grew into equiaxed grains with typical annealed twins during solution treatment. The addition of Cr and Zr refines the microstructure after solution treatment. The addition of Cr element separately has the minimal effect, followed by Zr addition separately, and co-addition of Cr and Zr elements has the best effects on grain refinement. The SEM micrographs of designed Cu-Ni-Si-(Cr-Zr) alloys after solution treatment are shown in Fig. 5. It can be seen that precipitates are absent in both the interior and boundaries of the grains for Cu-Ni-Si alloy, indicating complete solid solution of solutes. With Cr and Zr additions, the intermetallic particles formed during solidification remain after solution treatment. These particles could act as barriers for grain boundary migration by Zener pinning. According to the Zener's Equation, the pinning pressure of particles can be expressed as [25].

$$Z_p = \frac{3\gamma_{DB}F_v}{2r} \quad (1)$$

Where γ_{DB} is the energy per unit area for a high angle boundary, F_v is the volume fraction of particles and r is the radius. Apart from the slight difference in size and morphology, the main difference of intermetallic particles between Cu-Ni-Si-Cr and Cu-Ni-Si-Zr alloy is their distribution. The Cr_3Si particles lie inside the grains and exhibit consecutive necklace-like morphology with smooth boundaries, whereas the Ni_2SiZr particles mainly segregate at grain boundaries and show more characteristics of polygons with sharp edges. This indicates that during the recrystallization process, grain boundaries moved across Cr_3Si particles, but were pinned by Ni_2SiZr particles. As a result, Cu-Ni-Si-Zr alloy exhibits better refining effects than Cu-Ni-Si-Cr alloy. As for Cu-Ni-Si-Cr-Zr alloy, the finer grains are attributed to more Cr solutes in the matrix which reduces the mobility of grain migration compared with Cu-Ni-Si-Zr alloy.

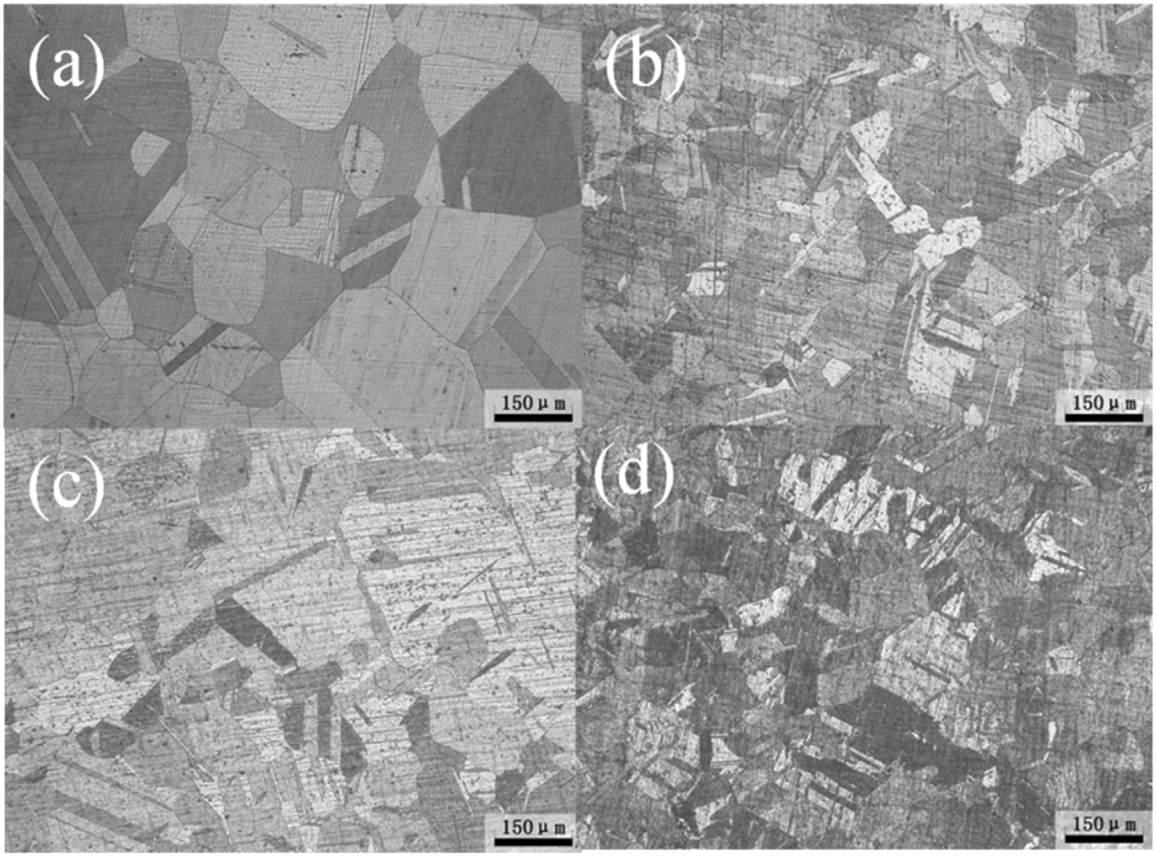

Fig. 4. Optical microstructure of designed Cu-Ni-Si-(Cr-Zr) alloys after solution treatment: (a) Cu-Ni-Si alloy; (b) Cu-Ni-Si-Zr alloy; (c) Cu-Ni-Si-Cr alloy; (d) Cu-Ni-Si-Cr-Zr alloy.

3.1.2. Microstructure of aged samples

Bright field TEM micrographs of designed Cu-Ni-Si-(Cr-Zr) alloys are shown in Fig. 6. Numerous nano-scaled precipitates can be observed. With Cr and Zr alloying, the grains are significantly refined and more sub-grains appear in the field of view. Meanwhile, extended dislocations nodes (showing the "Y" shape) introduced by heavy cold working are observed within the refined grains, as indicated by the arrows. It should be noted that with more sub-grains, the precipitates tend to form at sub-grain boundaries and dislocations owing to lower nucleation energy.

Fig. 7 illustrates dark field TEM image and corresponding selected area electron diffraction (SAED) pattern along $[001]_{Cu}$ of Cu-Ni-Si alloy aged at 773 K for 2 h. The mean diameter of precipitates is 5.2 nm according to Fig. 7(a). The indexed patterns in Fig. 7 (b) confirm the existence of Cu and δ-Ni_2Si phase in the specimen. Cu has face center cubic (FCC) structure, a=3.615 nm, and δ-Ni_2Si phase has orthorhombic structure, a=0.706 nm, b=0.499 nm, c=0.372 nm [26]. The reflection spots in Fig. 7(b) is slightly streaked, which is attributed to the strain arising in the matrix due to the formation of the ordered product phase in a very fine state of subdivision [27].

Fig. 8 illustrates the TEM images of Cu-Ni-Si-Zr alloy aged at 773 K for 2 h. Elongated grains with dislocations and deformation twins are observed. The high resolution transmission electron microscopy (HRTEM) analysis of twins indicates precipitation at twin-matrix boundaries and stacking faults induced by stress near twin boundaries (Fig. 11(b)). The precipitate occupying both matrix and twins is marked by circle and corresponding fast Fourier transformation (FFT) image indicates the presence of δ-Ni_2Si phase. The formation of δ-Ni_2Si phase can be attributed to lower nucleation energy at defects, which refers to the twin-matrix interface on this occasion. In ternary alloying, addition of a small amount of Zr is effective in introducing the stacking faults [23] and the SFE of Cu-Ni-Si alloy is lowered by Zr alloying. The critical twin nucleus thickness, λ_c, is correlated to the twin boundary energy (γ_{TB}) by the following equation [28].

$$\lambda_c = \frac{5\pi\rho G\gamma_{TB}}{2\sigma^2} \tag{2}$$

Where G is the shear modulus, ρ is the ratio of thickness to diameter of the twin embryo (a constant), γ_{TB} is the twin boundary energy, which is proportional to the SFE, and σ is the driving stress of twin nucleation. Hence, the critical twin nucleus thickness λ_c is proportional to γ_{TB}, which is proportional to the SFE. Lowering of SFE reduces the critical twin nucleus thickness, hence promoting the formation of deformation twins in Cu-Ni-Si-Zr alloy. The morphology of the intermetallic particles and corresponding SAED Pattern are shown in Fig. 8(c), near-elliptic particle with a major axis of 712 nm and a minor axis of 476 nm is observed. The results of energy dispersive X-ray (EDX) indicate the composition of Cu, Ni, Si and Zr, which is consistent with EDS results in Fig. 2.

Fig. 9 illustrates TEM images of Cu-Ni-Si-Cr alloy aged at 773 K for 2 h. HRTEM image (Fig. 9(a)) shows basket-weave structure with fine precipitates. The FFT image of marked area in Fig. 9(a) is shown in Fig. 9(b), in which δ-Ni_2Si phase is indexed. Moreover, superlattice spots around spots representing FCC copper matrix are observed, which indicates the occurrence of spinodal decomposition [29]. Fig. 9(c) illustrates spherical particles with a diameter of 340 nm and corresponding SAED patterns. The coarse particle is indexed as cubic Cr_3Si phase, a=0.4558 nm, which is confirmed by EDX results showing Cu, Cr and Si composition. The Cr_3Si phase is mainly formed during melting and solidification. Although Cr_3Si phase contribute little to the hardening of the

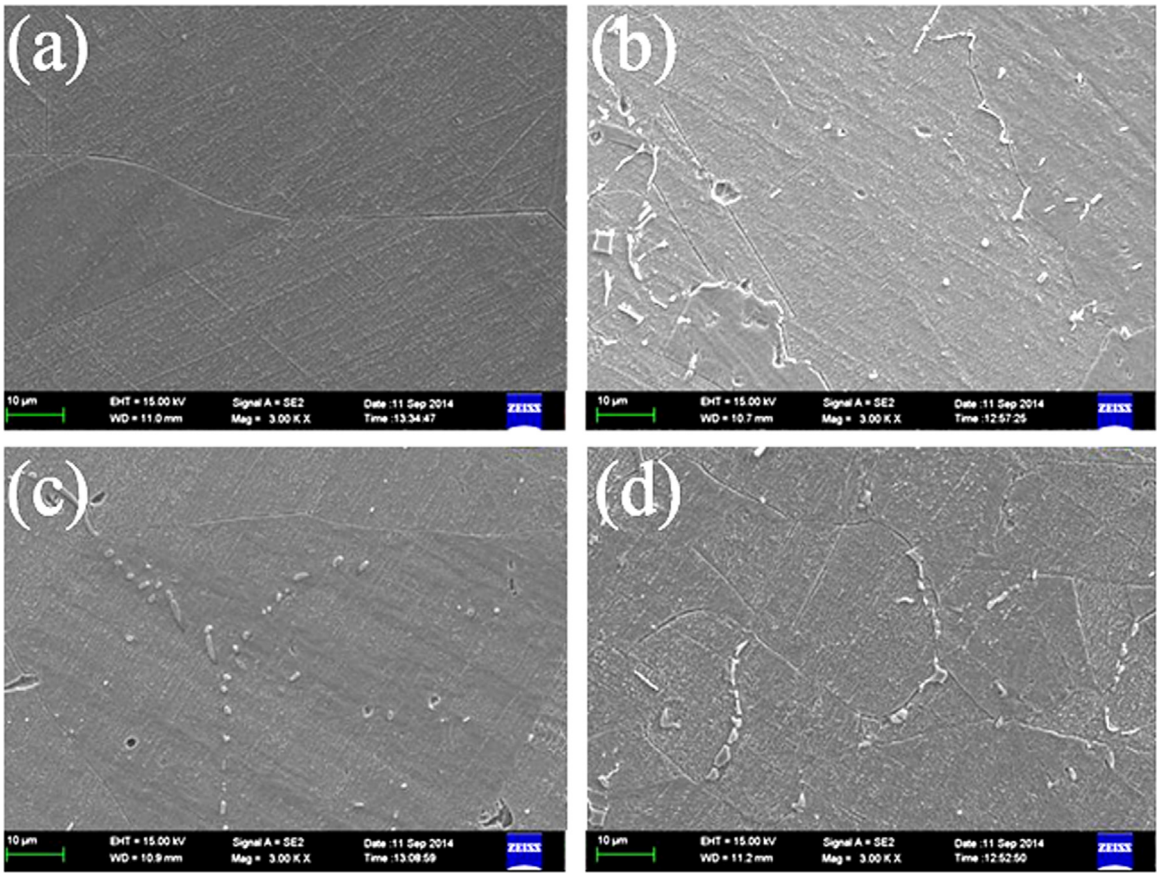

Fig. 5. SEM micrographs of designed Cu-Ni-Si-(Cr-Zr) alloys after solution treatment: (a) Cu-Ni-Si alloy; (b) Cu-Ni-Si-Zr alloy; (c) Cu-Ni-Si-Cr alloy; (d) Cu-Ni-Si-Cr-Zr alloy.

alloys, it can improve primarily the high temperature stability and impede grain growth during heating [30].

3.1.3. Fracture

In order to better understand the deformation behavior, the fracture surface of designed Cu-Ni-Si-(Cr-Zr) alloys are compared in Fig. 10. Quasi-cleavage ruptures appear in the Cu-Ni-Si alloy with tear ridges and fine shallow dimples of uniform distribution. Fine Ni_2Si precipitates can be observed at the bottom of dimples. With Cr and Zr alloying, typical dimple ruptures with bimodal distribution of dimples can be observed. The microstructure is composed of large deep dimples and fine shallow dimples. The homogeneity of Cu-Ni-Si alloy is spoiled by the intermetallic particles (Cr_3Si and Ni_2SiZr) produced by Cr and Zr elements, which accounts for the change of ruptures from quasi-cleavage to dimple. The intermetallic particles serve as nucleating sites of dimples during loading, resulting in the large dimples.

3.2. Properties

3.2.1. Hardness and electrical conductivity

Fig. 11 shows the variation of hardness and electrical conductivity of designed Cu-Ni-Si-(Cr/Zr) alloys versus temperature upon ageing for 1 h. The hardness of designed alloys is close at lower aging temperature. With the increase of ageing temperature, the hardness reaches the maximum value at about 723 K, and decreases at higher temperature. The peak values of hardness are all obtained upon ageing at 723 K for 1 h. The values are 232, 217, 224 and 227 HV for raw Cu-Ni-Si alloy, Cu-Ni-Si-Zr alloy, Cu-Ni-Si-Cr alloy and Cu-Ni-Si-Cr-Zr alloy, respectively. Generally, the hardness of Cu-Ni-Si alloy is about 10 HV higher than Cu-Ni-Si-Cr and Cu-Ni-Si-Cr-Zr alloy, and 20 HV higher than Cu-Ni-Si-Zr alloy. However, once over aged, the hardness of Cu-Ni-Si-Cr-Zr alloy and Cu-Ni-Si-Cr alloy becomes close to Cu-Ni-Si alloy. As shown in Fig. 11(b), the electrical conductivity of Cu-Ni-Si-(Cr-Zr) alloys increases with the increase of temperature, and the addition of Cr and Zr alloy increases the electrical conductivity slightly at all temperatures. The electrical conductivity of Cu-Ni-Si-Zr alloy is the highest under 748 K and exceeded by Cu-Ni-Si-Cr alloy thereafter.

Fig. 12 shows the variation of hardness and electrical conductivity of cold rolled Cu-Ni-Si-(Cr/Zr) alloys against isothermal aging at 723 K and 773 K, respectively. When aged at 723 K, the hardness of tested alloys increases rapidly at the beginning and reaches the peak and then remains stable with slight decrease. The hardness of Cu-Ni-Si-Zr is the lowest in the full range, while the hardness of Cu-Ni-Si-Cr and Cu-Ni-Si-Cr-Zr alloy is lower at the beginning and exceeds Cu-Ni-Si alloy when aged for 180 min or more. Peak values are 232 HV for Cu-Ni-Si alloy ageing for 60 min, 217 HV for Cu-Ni-Si-Zr alloy ageing for 60 min, 232 HV for Cu-Ni-Si-Cr alloy ageing for 120 min and 229 HV for Cu-Ni-Si-Cr-Zr alloy ageing for 120 min. As shown in Fig. 12(b), the electrical conductivity of all tested alloys increases with the increase of ageing time, and the addition of Cr and Zr elements increases the electrical conductivity under all conditions. The electrical conductivity of Cu-Ni-Si-Zr alloy is the highest. When aged at 773 K, the hardness increases dramatically to reach the peak value and decreases dramatically thereafter. Peak values are 237 HV for Cu-Ni-Si alloy ageing for 10 min, 205 HV for Cu-Ni-Si-Zr alloy ageing for 30 min, 232 HV for Cu-Ni-Si-Cr alloy ageing for 30 min and 222 HV for Cu-Ni-Si-Cr-Zr alloy ageing for 30 min. The addition of Cr and Zr obviously retards the precipitation process. As for the variation of electrical conductivity, specimens aged at 773 K generally show the same trend as those aged at 723 K. The electrical conductivity increases with the increase of time and can be improved by the

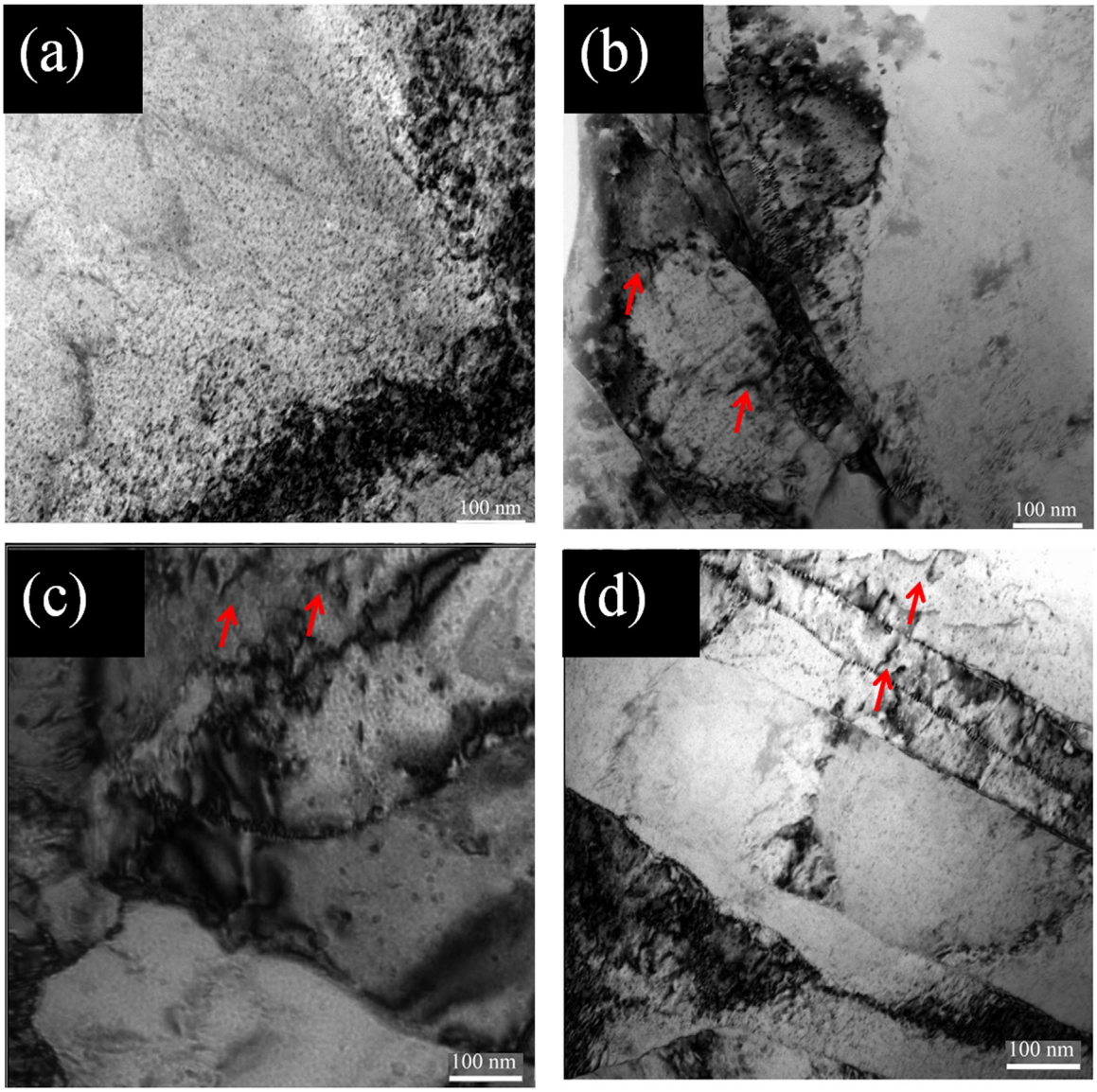

Fig. 6. TEM images of designed Cu-Ni-Si-(Cr-Zr) alloys aged at 773 K for 2 h: (a) Cu-Ni-Si alloy; (b) Cu-Ni-Si-Zr alloy; (c) Cu-Ni-Si-Cr alloy; (d) Cu-Ni-Si-Cr-Zr alloy.

addition of Cr and Zr elements. However, Cu-Ni-Si-Cr alloy exhibits the highest electrical conductivity when aged at 773 K instead of Cu-Ni-Si-Zr alloy.

3.2.2. *Comprehensive properties and comparisons*

Fig. 13 illustrates the engineering stress-strain of designed Cu-Ni-Si-(Cr-Zr) alloys. The comprehensive properties are shown in Table 2. The ultimate tensile strength of Cu-Ni-Si alloy is 625 MPa and the electrical conductivity is 47.1% IACS. Adding Zr element deteriorates the mechanical strength (587 MPa) with very little improvement in electrical conductivity (47.5% IACS). Adding Cr element and co-adding Cr and Zr elements both improve the mechanical strength and electrical conductivity at the same time. The ultimate strength reaches 700 and 706 MPa, and the electrical conductivity is 49.7% and 48.5% IACS, respectively. It's worth noting that the elongation of Cu-Ni-Si-Cr-Zr alloy reaches 9.5%, while Cu-Ni-Si-Cr alloy only reaches 6.6%.

The comparison of properties of various Cu-Ni-Si system alloys with designed Cu-Ni-Si-Cr-Zr alloy is shown in Table 3. It should be noted that alloys with a dominating composition of Cu-2.0 wt% Ni-0.5 wt%Si are employed. The Cu-Ni-Si-Mg [31] alloy shows better elongation but the ultimate strength reaches 630 MPa only. Both the ultimate strength and hardness of Cu-Ni-Si-Ti alloy exceeds designed Cu-Ni-Si-Cr-Zr alloy (710 MPa and 227 HV respectively) [32]. However, the elongation and electrical conductivity of Cu-Ni-Si-Ti alloy is relatively low. As for the Cu-Ni-Si-V alloy, the hardness reaches 202 HV, but the electrical conductivity is the lowest (42% IACS) [19]. The designed Cu-Ni-Si-Cr-Zr alloy possesses excellent comprehensive mechanical properties and relatively high electrical conductivity.

3.2.3. *Effects of Cr and Zr additions on mechanical properties of Cu-Ni-Si alloys*

It is suggested by earlier researchers that the yield stress of the Cu-Ni-Si system alloys containing δ-Ni_2Si precipitates at room temperature is controlled by the Orowan mechanism under peak-aging and over-aging conditions [33]. The Orowan stress is inversely proportional to the inter-precipitate spacing, λ [32]. The change in strength induced by Cr and Zr alloying can be discussed by estimating, λ, which is considered to be the square lattice spacing in parallel planes and written as [34].

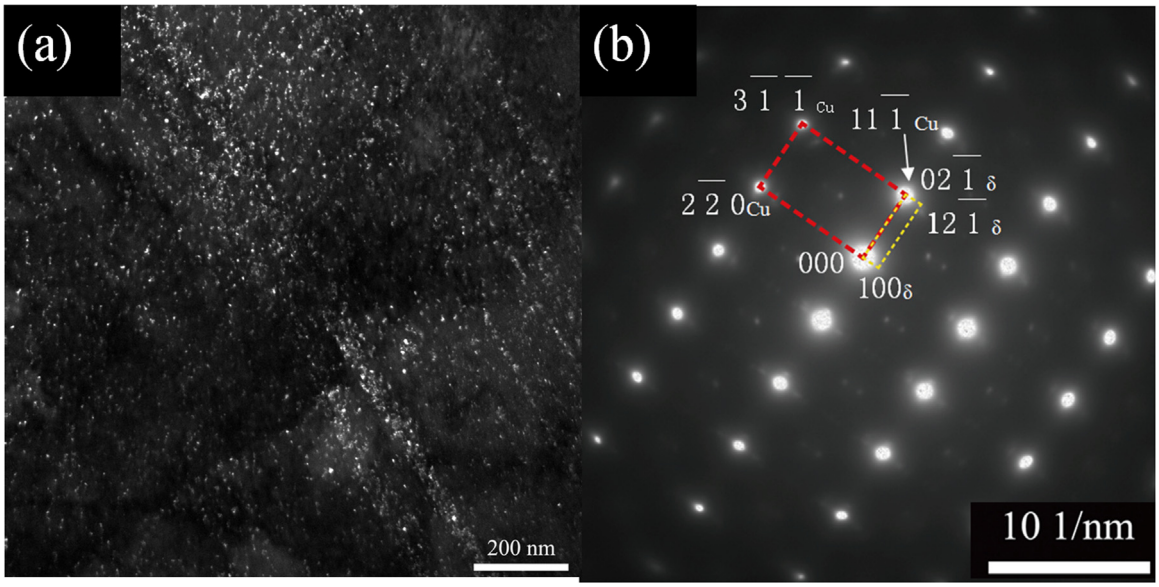

Fig. 7. Dark field TEM image (a) and corresponding SAED Pattern along $[001]_{Cu}$, (b) of Cu-Ni-Si alloy aged at 773 K for 2 h.

$$\lambda = r_0\left[\sqrt{\frac{2\pi}{3f}} - 1.63\right] \quad (3)$$

Where r_0 *is* the is the average radius of spherical precipitates and f is the volume fraction of precipitates. With the addition of Zr element, the amount of solutes in the matrix is reduced owing to the formation of Ni_2SiZr phase, which results in the decrease of precipitate volume fraction f. According to Eq. (3), λ increases when f decreases, and strengthening from Orowan looping mechanism is decreased. Owing to the larger solute limit of Cr in copper, the addition of Cr separately introduces additional Cr solutes into copper matrix despite the formation of Cr_3Si phase, thus increasing precipitate volume fraction f and promoting Orowan strengthening. As for co-addition of Cr and Zr elements, Zr reacts with Ni and Si to form Ni_2SiZr phase and Cr mainly dissolves into copper matrix (Fig. 2(d1)–(d5)). The amount of solutes is increased by Cr solutioning and Orowan strengthening is promoted as a result. Both Cr and Zr elements reduce the grain size of recrystallized grains during solution treatment and subsequently refine the microstructure after cold rolling. Strengthening from grain refinement is improved according to the Hall-Patch relationship [35]. However, the effect of grain refinement strengthening is minor compared to Orowan strengthening. Generally, the addition of Zr deteriorates mechanical strength, and addition of Cr separately and co-addition of Cr and Zr improve mechanical property.

As mentioned above, the addition of Zr results in the lowering of SFE, which would lead to the dissociation of screw dislocations into particles making cross-glide difficult. In other words, it means the alloy would be a planar-slip material in contrast to the wary-slip nature of pure copper [36]. As a result, better elongation is obtained with Zr additions. In addition, the addition of Zr shows significant grain refinement, which also promotes elongation. In this study, the designed Cu-Ni-Si-Zr exhibits best elongation (18.5%), and the elongation of Cu-Ni-Si-Cr-Zr alloy exceeds Cu-Ni-Si-Cr alloy (9.5–6.6%).

3.2.4. Effects of Cr and Zr additions on electrical conductivity of Cu-Ni-Si alloys

According to Matthiessen's rule, the electrical resistivity of metals is given by

$$\rho = \rho_s + \Delta\rho_I + \Delta\rho_D + \Delta\rho_P \quad (4)$$

Where ρ is the real resistivity, ρ_S, $\Delta\rho_I$, $\Delta\rho_D$ and $\Delta\rho_P$ are the resistivity sourcing from solute atoms, dislocations, interfaces and phonon scattering respectively. Solution scattering is dependent on the amount of solution atoms, which is the dominating factor for substitutional alloys. Phonon scattering sources from thermal vibrations and is dependent on temperature. Thus $\Delta\rho_P$ take a constant value as all electrical conductivity tests were performed at 293 K. Dislocation scattering is dependent on the dislocation density. Interface scattering is dependent on the amount of interfaces. With Cr and Zr additions, new particle-matrix interfaces are introduced by Cr_3Si and Ni_2SiZr particles and more grain boundaries arise due to grain refinement. As a result, interface scattering is prompted. However, the influence of interface scattering is minor compared to solution scattering. The Effects of Cr and Zr addition on electrical conductivity of Cu-Ni-Si alloys is discussed on the basis of solution scattering.

Table 4 illustrates the electrical conductivity of designed Cu-Ni-Si-(Cr-Zr) alloy in different states. In solution treated states, the electrical conductivity of Cu-Ni-Si-Zr alloy is improved owing to the formation of Ni_2SiZr phase, which reduces the amount of Ni and Si solutes. However, the influence of Cr element is quite different. During solidification, part of the added Cr elements reacts with Si to form Cr_3Si particles, while the rest dissolves into copper matrix. The overall amount of solutes is increased and electrical conductivity is deteriorated. For Cu-Ni-Si-Cr-Zr alloy, Zr element reacts with Ni and Si to form Ni_2SiZr particles and Cr element dissolves into copper matrix, which results in the decrease in electrical conductivity. In the subsequent cold rolling, numerous dislocations are generated and the electrical conductivity of all tested alloys is slightly decreased due to the increased dislocation scattering. During ageing, solute atoms precipitate from copper matrix and the electrical conductivity is significantly improved. Due to the reduced dissolution limits of Cr in copper, Cr element precipitates upon ageing and reduces the amount of solutes in the matrix. As a result, the electrical conductivity of Cu-Ni-Si-Cr and Cu-Ni-Si-Cr-Zr alloy exceeds Cu-Ni-Si alloy after ageing treatment.

3.3. Precipitation kinetics

The kinetics of precipitation can be empirically expressed by

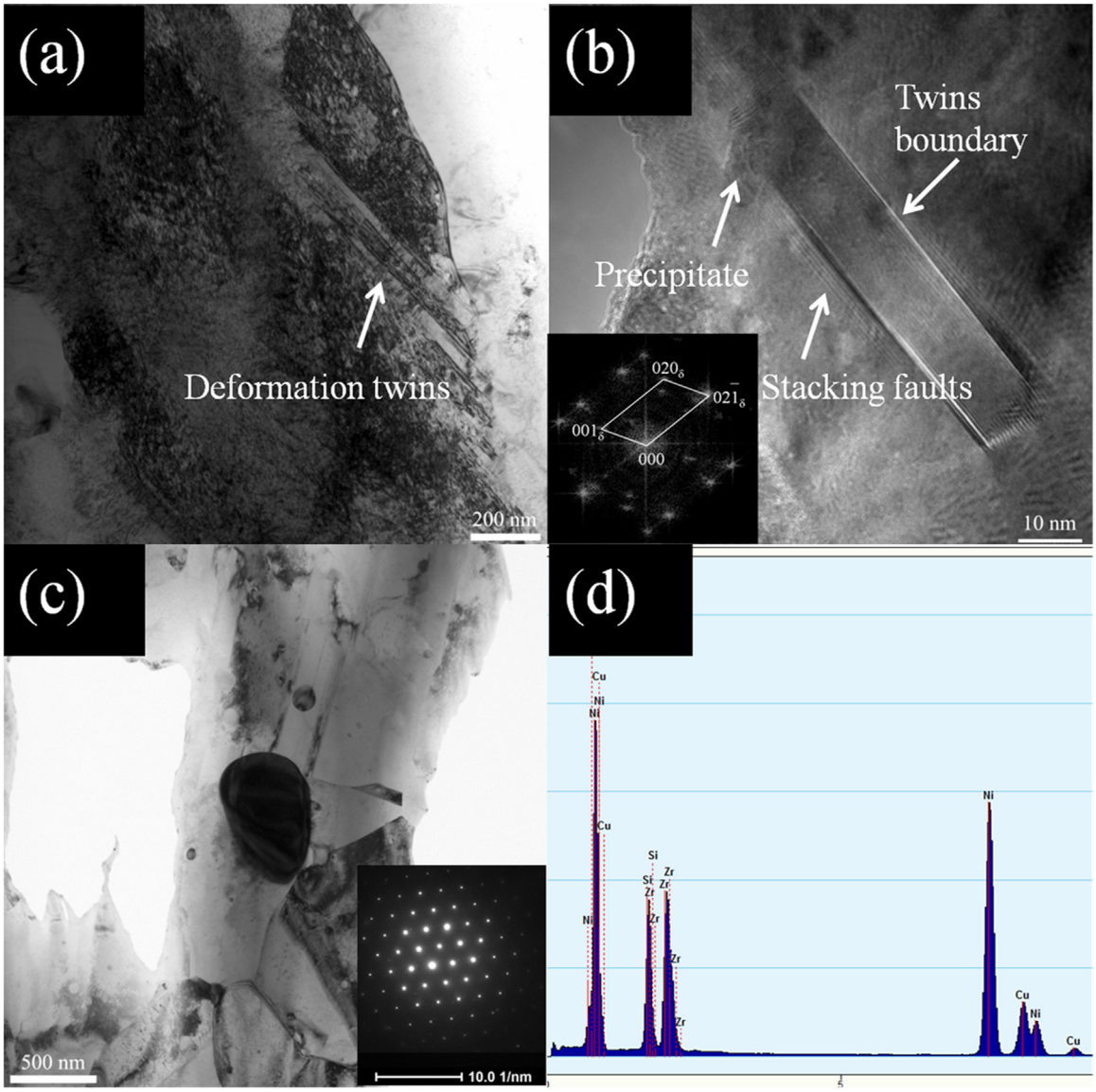

Fig. 8. TEM images of Cu-Ni-Si-Zr alloy aged at 773 K for 2 h: (a) bright field image showing twins; (b) HRTEM of twins with precipitates and corresponding FFT; (c) bright field image of coarse eutectic particles with SAED and corresponding EDX results (d).

the Avrami-equation:

$$X = 1 - \exp(-kt^n) \tag{5}$$

$$\ln(k) + n\ln(t) = \ln(\ln(1/(1 - X))) \tag{6}$$

Where k is a constant depending on temperature, composition of supersaturated solid solution and grain size, and n is a constant depending on the type of phase transformation and nucleation. During aging at certain temperature, solute atoms precipitate from supersaturated solid solution to form precipitate particles. The volume fraction of precipitates, X, can be expressed as

$$X = \frac{V}{V_{max}} \tag{7}$$

Where V is the volume of precipitates formed in unit volume at given time t and V_{max} is the maximum volume of precipitates that can be precipitate formed in unit volume at certain temperature, which is equal to the balance volume in thermal dynamics. According to the simplified Matthiessen's law, there's a linear relationship between electrical conductivity and volume fraction of precipitates for solid solutions. Thus the electrical conductivity C at given time t is expressed as

$$C = C_0 + (C_{max} - C_0)\cdot X \tag{8}$$

Where C_0 is the electrical conductivity at the very beginning of precipitation and C_{max} is the maximum electrical conductivity, which corresponds with V_{max}. Solve Eq. (8) for X, the volume fraction of precipitates X can be expressed as

$$X = \frac{C - C_0}{C_{max} - C_0} \tag{9}$$

Therefore, the volume fraction of precipitates at given time, t, could be obtained through measurements of electrical conductivity. In the present study, the alloys were casted, homogenized, hot-rolled, solution treated, cold rolled and finally aged. Neglecting natural aging at room temperature, C_0 takes the value of alloys in the cold rolled state, and C_{max} takes the value of alloys aged for enough time (240 min for ageing at 723 K and 180 min for ageing at 773 K). The electrical conductivity and volume fraction of

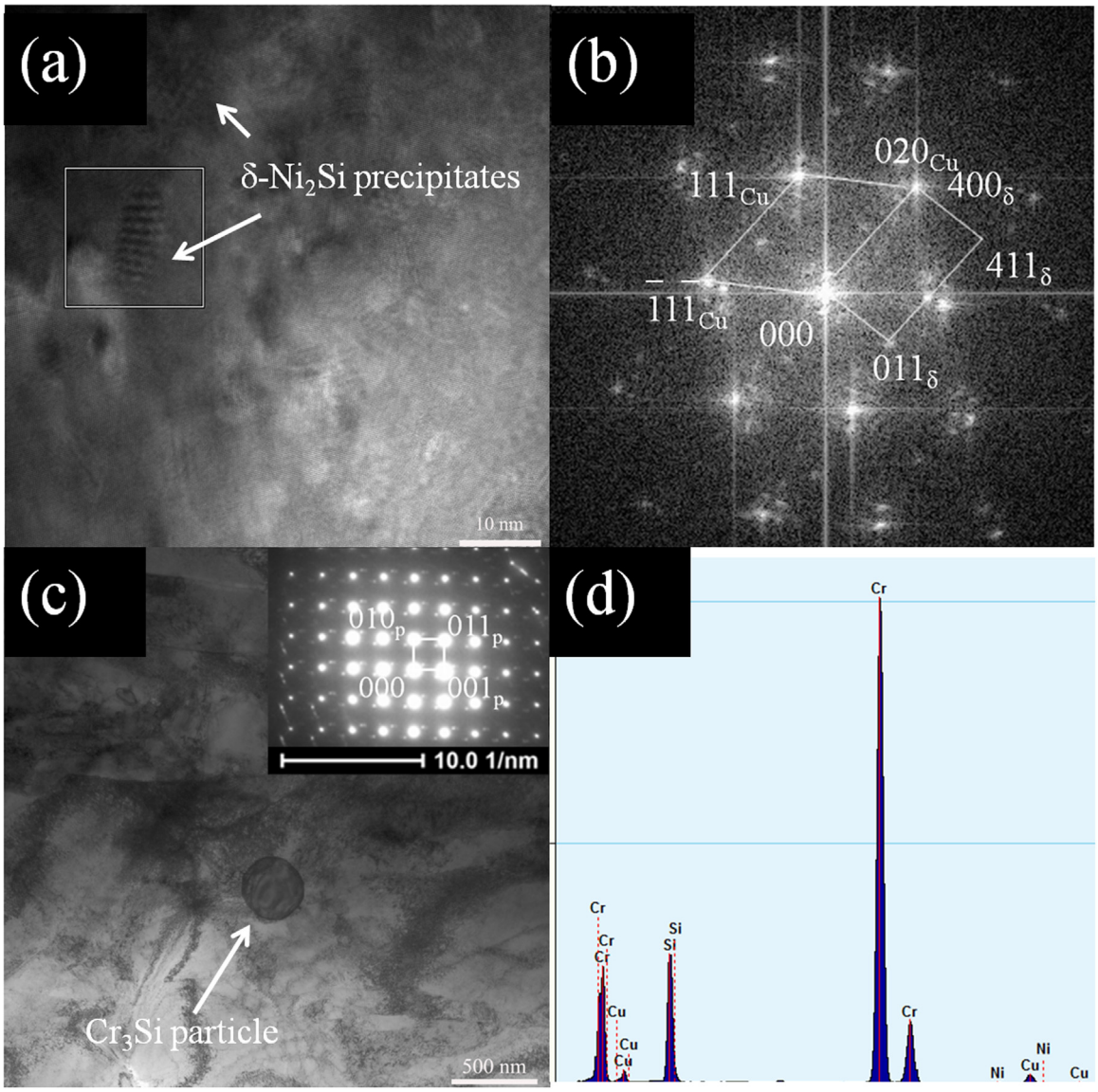

Fig. 9. TEM images of Cu-Ni-Si-Cr alloy aged at 773 K for 2 h: (a) HRTEM showing precipitates; (b) FFT image of marked area in (a); (c) bright field image of eutectic particles, the inset in (c) is corresponding SAED Pattern; (d) corresponding EDX results of (c).

precipitates of designed Cu-Ni-Si-Cr-Zr alloys aged at 723 K and 773 K are shown in Tables 5 and 6 respectively.

Fig. 14 presents plots of ln (ln (1/(1−X))) versus ln (t) utilizing data of t and X in Tables 5 and 6. The values of k and n can be obtained from the linear fitting of plots according to Eq. (6). The calculated kinetic Avrami equations of designed Cu-Ni-Si-(Cr/Zr) alloys for precipitation are listed in Table 7. When the ageing temperature increases from 723 K to 773 K, the values of k for all alloys are increased, which is consistent with accelerated precipitation process due to enhanced diffusion at higher temperatures.

According to Arrhenius equation, the precipitation rate of Ni_2Si is expressed as

$$\frac{\partial X}{\partial t}=A\exp\left(-\frac{E_a}{RT}\right) \tag{10}$$

Where A is the pre-exponential factor which can be taken as a constant, E_a is the activation energy and R is the gas constant. Integrate Eq. (11) and solve for E_a, the activation energy can be obtained by

$$E_a = -R\left[\partial\left(\ln\left(\partial X/\partial t\right)\right)/\partial\left(1/T\right)\right]_{X_{0.01}} \tag{11}$$

Where the volume fraction of precipitates $X=0.01(1\%)$ is taken as the beginning of precipitation and ln $(\partial X/\partial t)$ is calculated from kinetic equations in Table 7. The plot of ln $(\partial X/\partial t)$ against $1/T$ is shown in Fig. 15 and $\partial(\ln(\partial X/\partial t)/\partial(1/T))$ can be obtained from the slope. According to Eq. (11), the calculated activation energies for Ni_2Si precipitation are 105 kJ/mol for Cu-Ni-Si alloy, 89 kJ/mol for Cu-Ni-Si-Zr alloy, 115 kJ/mol for Cu-Ni-Si-Cr alloy and 111 kJ/mol for Cu-Ni-Si-Cr-Zr alloy. Our results are reliable compared with previous studies. The volume diffusion activation energies of Cu, Ni and Si in copper are 211, 236 and 172 kJ/mol respectively [37]. Donoso studied a Cu–2.8Ni–1.4Si (at%) alloy through microcalorimetric analysis and the calculated activation energy for the precipitation of δ-Ni_2Si was 108 kJ/mol [38]. Shinji studied the microstructure of a forged Cu-4.2Ni-1.0Si (at%) alloy determined the activation energies for Ni_2Si precipitation as 124 kJ/mol for Cu-Ni-Si alloy [37]. The difference may be attributed the composition imparity and different deformation degrees. The addition of Zr reduces the activation energy of Ni_2Si precipitation for Cu-Ni-Si alloy, whereas the addition of Cr and co-addition of Cr and Zr increase the value of it. It is worth to be noted

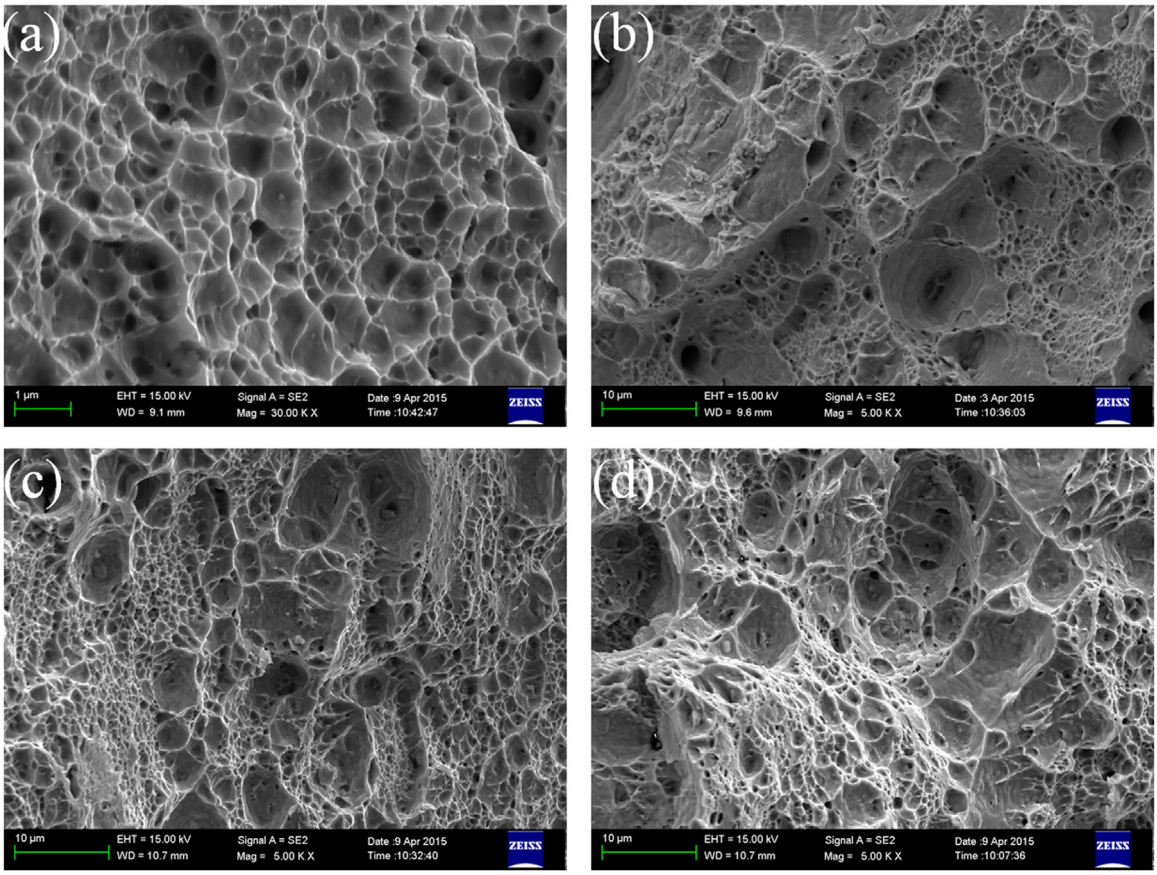

Fig. 10. Fracture surface of designed Cu-Ni-Si-(Cr-Zr) alloys: (a) Cu-Ni-Si alloy; (b) Cu-Ni-Si-Zr alloy; (c) Cu-Ni-Si-Cr alloy; (d) Cu-Ni-Si-Cr-Zr alloy.

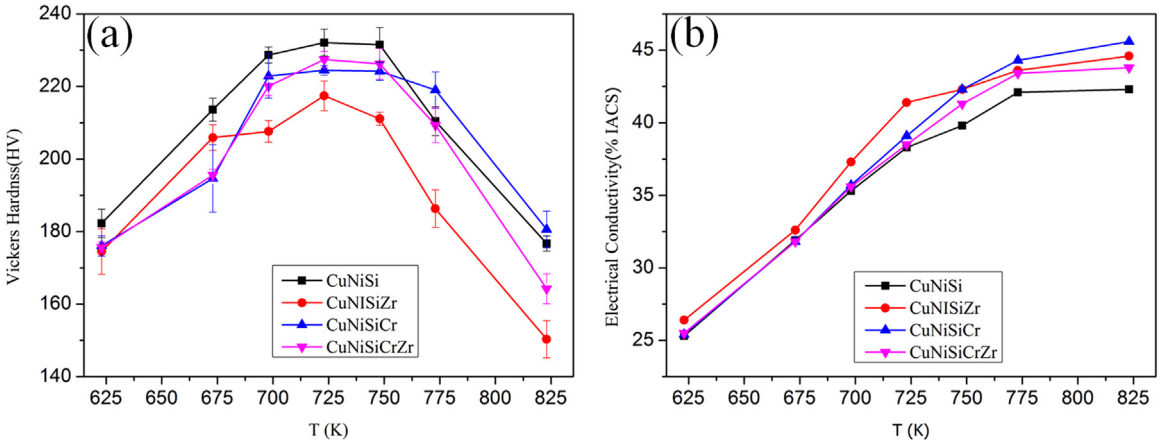

Fig. 11. Variation of hardness and electrical conductivity of designed Cu-Ni-Si-(Cr-Zr) alloys versus temperature upon ageing for 1 h.

that increased the activation energy of co-addition of Cr and Zr is lower than that of Cr addition.

4. Conclusions

(1) The addition of Cr and Zr results in formation of Cr_3Si and Ni_2SiZr intermetallic compounds, respectively, thus increases the electrical conductivity of Cu-Ni-Si alloy and refines the microstructure.

(2) Alloying with Zr element deteriorates mechanical strength of Cu-Ni-Si alloy, whereas in the presence of Cr, to the contrary, the ultimate tensile strength is increased, whether Zr is incorporated or not.

(3) Microstructure analysis confirms the presence of δ-Ni_2Si precipitates, which strengthens the alloy through Orowan mechanism.

(4) According to Avrami equation, the calculated activation energies of precipitation are 105, 89, 115 and 111 kJ/mol for Cu-Ni-Si, Cu-Ni-Si-Zr, Cu-Ni-Si-Cr and Cu-Ni-Si-Cr-Zr alloy, respectively.

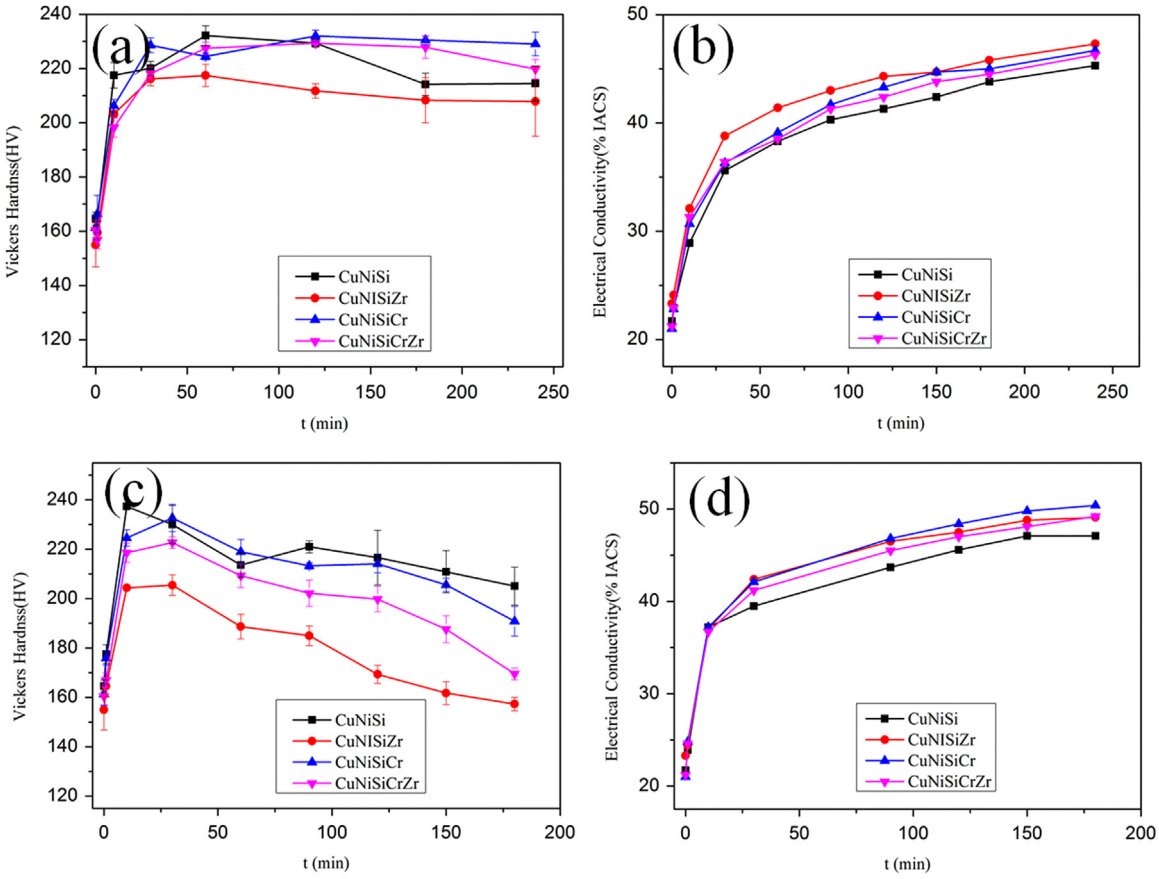

Fig. 12. Variation of hardness and electrical conductivity of designed Cu-Ni-Si-(Cr-Zr) alloys aged at 723 K (a and b) and 773 K (c and d).

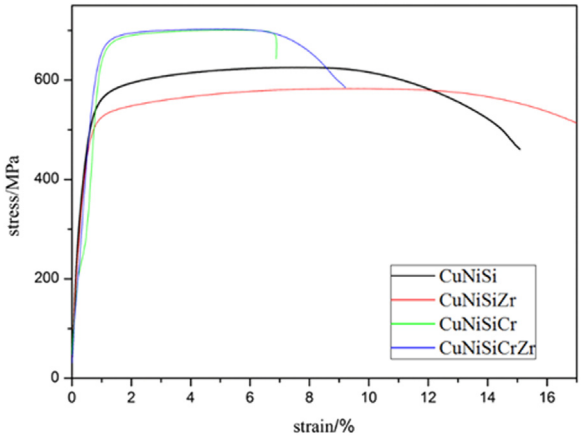

Fig. 13. Engineering stress versus strain of designed Cu-Ni-Si-(Cr-Zr) alloys.

Table 2
Comprehensive properties of designed Cu-Ni-Si-(Cr/Zr) alloys.

	UTS/MPa	δ/%	Electrical conductivity/(% IACS)	Vickers Hardness
Cu-Ni-Si	625	15.1	47.10	189.4
Cu-Ni-Si-Zr	587	18.5	47.50	168.3
Cu-Ni-Si-Cr	700	6.6	49.70	212.5
Cu-Ni-Si-Cr-Zr	706	9.5	48.20	208.8

Table 3
Comparison of properties of various Cu-Ni-Si system alloys with designed Cu-Ni-Si-Cr-Zr alloy.

	σ_{UTS}/MPa	δ/%	Electrical conductivity/(% IACS)	Vickers Hardness
Cu-Ni-Si-Cr-Zr	706	9.2	48.2	208.8
Cu-Ni-Si-Mg	630	11	44	/
Cu-Ni-Si-Ti	710	6	45.1	227
Cu-Ni-Si-V	/	/	42	202

Table 4
Electrical conductivity of designed Cu-Ni-Si-(Cr-Zr) alloy in different states.

	Cu-Ni-Si	Cu-Ni-Si-Zr	Cu-Ni-Si-Cr	Cu-Ni-Si-Cr-Zr
Solution treated/(%IACS)	22.0	23.6	21.6	21.4
Cold rolled/(%IACS)	21.7	23.3	21	21.2
723 K Aged for 180 min/(% IACS)	43.8	45.8	45	44.5

(5) The best integrated performance is obtained through co-addition of Cr and Zr elements. The ultimate strength, elongation and electrical conductivity are 706 MPa, 9.5% and 48.2% IACS, respectively.

Table 5
Electrical conductivity (C) and volume fraction of precipitates (X) of designed Cu-Ni-Si-(Cr/Zr) alloys aged at 723 K for different time.

t/min	Cu-Ni-Si		Cu-Ni-Si-Zr		Cu-Ni-Si-Cr		Cu-Ni-Si-Cr-Zr	
	C/%IACS	X/%	C/%IACS	X/%	C/%IACS	X/%	C/%IACS	X/%
0	21.7	0	23.3	0	21	0	21.2	0
1	22.9	5.08	24.1	3.33	22.8	7.00	22.9	6.77
10	28.9	30.51	32.1	36.67	30.7	37.74	31.3	40.24
30	35.6	58.90	38.8	64.58	36.3	59.53	36.4	60.56
60	38.3	70.34	41.4	75.42	39.1	70.43	38.5	68.92
90	40.3	78.81	43	82.08	41.7	80.54	41.3	80.08
120	41.3	83.05	44.3	87.50	43.3	86.77	42.4	84.46
150	42.4	87.71	44.7	89.17	44.7	92.22	43.8	90.04
180	43.8	93.64	45.8	93.75	45	93.39	44.5	92.83
240	45.3	100.00	47.3	100.00	46.7	100.00	46.3	100.00

Table 6
Electrical conductivity (C) and volume fraction of precipitates (X) of designed Cu-Ni-Si-(Cr/Zr) alloys aged at 773 K for different time.

t/min	Cu-Ni-Si		Cu-Ni-Si-Zr		Cu-Ni-Si-Cr		Cu-Ni-Si-Cr-Zr	
	C/%IACS	X/%	C/%IACS	X/%	C/%IACS	X/%	C/%IACS	X/%
0	21.7	0	23.3	0	21	0	21.2	0
1	23.9	8.66	24.4	4.26	24.8	12.93	24.6	12.14
10	37.2	61.02	37	53.10	37.2	55.10	36.7	55.36
30	39.5	70.08	42.4	74.03	42.1	71.77	41.2	71.43
90	43.7	86.61	46.5	89.92	46.8	87.76	45.5	86.79
120	45.6	94.09	47.5	93.80	48.4	93.20	47	92.14
150	47	99.61	48.8	98.84	49.8	97.96	48.1	96.07
180	47.1	100.00	49.1	100.00	50.4	100.00	49.2	100.00

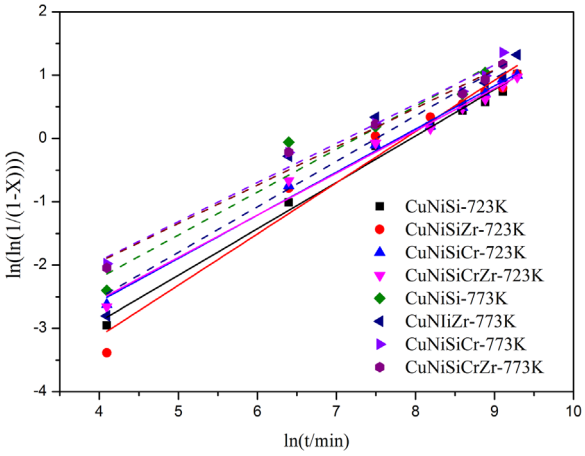

Fig. 14. Plots of ln (ln (1/(1 − X))) against ln (t) of designed Cu-Ni-Si-(Cr-Zr) alloys aged at 723 K and 773 K.

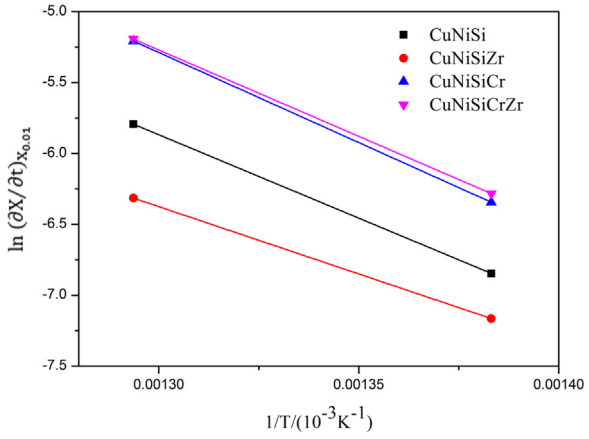

Fig. 15. Plots of ln (∂X/∂t) against 1/T of designed Cu-Ni-Si-(Cr-Zr) alloys.

Table 7
Kinetic Avrami equations of designed Cu-Ni-Si-(Cr/Zr) alloys aged at 723 K and 773 K.

Alloy	723 K	773 K
CuNiSi	$1-\exp(-0.003t^{0.73})$	$1-\exp(-0.0074t^{0.68})$
CuNiSiZr	$1-\exp(-0.0017t^{0.81})$	$1-\exp(-0.0046t^{0.72})$
CuNiSiCr	$1-\exp(-0.005t^{0.68})$	$1-\exp(-0.0122t^{0.62})$
CuNiSiCrZr	$1-\exp(-0.0054t^{0.67})$	$1-\exp(-0.0126t^{0.61})$

Acknowledgments

The authors gratefully acknowledge the supports of National Natural Science Foundation of China (Nos. 51525401, 51274054, U1332115, 51401044, U1432104), the China Postdoctoral Science Foundation (2015M581331), and the Fundamental Research Funds for the Central Universities. The authors wish to thank all the staff members of the 4B9A beamline of BSRF for corresponding experiments and discussion.

References

[1] C.D. Xia, W. Zhang, Z.Y. Kang, Y.L. Jia, Y.F. Wu, R. Zhang, G.Y. Xu, M.P. Wang, High strength and high electrical conductivity Cu–Cr system alloys manufactured by hot rolling–quenching process and thermomechanical treatments, Mater. Sci. Eng.: A 538 (2012) 295–301.
[2] W. Zhai, W.L. Wang, D.L. Geng, B. Wei, A DSC analysis of thermodynamic properties and solidification characteristics for binary Cu–Sn alloys, Acta Mater. 60 (2012) 6518–6527.
[3] R.G. Li, H.J. Kang, Z.N. Chen, G.H. Fan, C.L. Zou, W. Wang, S.J. Zhang, Y.P. Lu, J. C. Jie, Z.Q. Cao, A promising structure for fabricating high strength and high electrical conductivity copper alloys, Sci. Rep. 6 (2016).
[4] T. Sakai, H. Miura, N. Muramatsu, Effect of small amount addition of Co on dynamic recrystallization of Cu-Be alloys, Mater. Trans., JIM 36 (1995) 1023–1030.

[5] Y. Pang, C.D. Xia, M.P. Wang, Z. Li, Z. Xiao, H.G. Wei, X.F. Sheng, Y.L. Jia, C. Chen, Effects of Zr and (Ni, Si) additions on properties and microstructure of Cu–Cr alloy, J. Alloy. Compd. 582 (2014) 786–792.
[6] R. Mahmudi, A. Karsaz, A. Akbari-Fakhrabadi, A.R. Geranmayeh, Impression creep study of a Cu–0.3Cr–0.1Ag alloy, Mater. Sci. Eng.: A 527 (2010) 2702–2708.
[7] C. Watanabe, R. Monzen, K. Tazaki, Mechanical properties of Cu–Cr system alloys with and without Zr and Ag, J. Mater. Sci. 43 (2008) 813–819.
[8] D.-P. Lu, J. Wang, W.-J. Zeng, Y. Liu, L. Lu, B.-D. Sun, Study on high-strength and high-conductivity Cu–Fe–P alloys, Mater. Sci. Eng.: A 421 (2006) 254–259.
[9] Q. Lei, Z. Li, T. Xiao, Y. Pang, Z.Q. Xiang, W.T. Qiu, Z. Xiao, A new ultrahigh strength Cu–Ni–Si alloy, Intermetallics 42 (2013) 77–84.
[10] V.C. Srivastava, A. Schneider, V. Uhlenwinkel, K. Bauckhage, Effect of thermomechanical treatment on spray formed Cu–Ni–Si alloy, Mater. Sci. Technol. 20 (2004) 839–848.
[11] A. Araki, E. Kobayashi, T. Sato, W. Poole, Deformation Twinning Behavior in Precipitate Strengthened Cu-Ni-Si Alloys, John Wiley & Sons, Inc, Hoboken, NJ, USA, 2015.
[12] X.G. Zhang, J.N. Han, L. Chen, B.W. Zhou, Y.Y. Xue, F. Jia, Effects of B and Y additions on the microstructure and properties of Cu-Mg-Te alloys, J. Mater. Res. 28 (2013) 2747–2752.
[13] Z. Sun, C. Laitem, A. Vincent, Dynamic embrittlement at intermediate temperature in a Cu–Ni–Si alloy, Mater. Sci. Eng. A 477 (2008) 145–152.
[14] S.C. Krishna, J. Srinath, A.K. Jha, B. Pant, S.C. Sharma, K.M. George, Microstructure and Properties of a High-Strength Cu-Ni-Si-Co-Zr Alloy, J. Mater. Eng. Perform. 22 (2013) 1–6.
[15] G. Li, B.G. Thomas, J.F. Stubbins, Modeling creep and fatigue of copper alloys, Metall. Mater. Trans. A 31 (2000) 2491–2502.
[16] Q.S. Wang, G.L. Xie, X.J. Mi, B.Q. Xiong, X.P. Xiao, The precipitation and strengthening mechanism of Cu-Ni-Si-Co alloy, Mater. Sci. Forum (2013) 294–298.
[17] A. Ozawa, C. Watanabe, R. Monzen, Influence of Co on strength of Cu-Ni-Co-Si alloy, Mater. Sci. Forum (2014) 2468–2473.
[18] C. Watanabe, F. Nishijima, R. Monzen, K. Tazaki, Mechanical properties of Cu-4.0 wt%Ni-0.95 wt%Si alloys with and without P and Cr addition, Mater. Sci. Forum (2007) 2321–2324.
[19] S.Z. Han, J.H. Gu, J.H. Lee, Z.P. Que, J.H. Shin, S.H. Lim, S.S. Kim, Effect of V addition on hardness and electrical conductivity in Cu-Ni-Si alloys, Met. Mater. Int. 19 (2013) 637–641.
[20] H.G. Kim, T.W. Lee, S.M. Kim, S.Z. Han, K. Euh, W.Y. Kim, S.H. Lim, Effects of Ti addition and heat treatments on mechanical and electrical properties of Cu-Ni-Si alloys, Met. Mater. Int. 19 (2013) 61–65.
[21] Y.X. Ye, X.Y. Yang, J. Wang, X.K. Zhang, Z.L. Zhang, T. Sakai, Enhanced strength and electrical conductivity of Cu–Zr–B alloy by double deformation–aging process, J. Alloy. Compd. 615 (2014) 249–254.
[22] M. Azimi, G.H. Akbari, Development of nano-structure Cu-Zr alloys by the mechanical alloying process, J. Alloy. Compd. 509 (2011) 27–32.
[23] K. Kapoor, D. Lahiri, I.S. Batra, S.V.R. Rao, T. Sanyal, X-ray diffraction line profile analysis for defect study in Cu-1 wt% Cr-0.1 wt% Zr alloy, Mater. Charact. 54 (2005) 131–140.
[24] W.H. Sun, H.H. Xu, S.H. Liu, Y. Du, Z.H. Yuan, B.Y. Huang, Phase equilibria of the Cu–Ni–Si system at 700 °C, J. Alloy. Compd. 509 (2011) 9776–9781.
[25] F. Humphreys, M. Hatherly, Recrystallization and related annealing Phenomena, 2004.
[26] T. Hu, J.H. Chen, J.Z. Liu, Z.R. Liu, C.L. Wu, The crystallographic and morphological evolution of the strengthening precipitates in Cu–Ni–Si alloys, Acta Mater. 61 (2013) 1210–1219.
[27] J.Y. Cheng, B. Shen, F.X. Yu, Precipitation in a Cu–Cr–Zr–Mg alloy during aging, Mater. Charact. 81 (2013) 68–75.
[28] Y. Zhang, N.R. Tao, K. Lu, Effect of stacking-fault energy on deformation twin thickness in Cu–Al alloys, Scr. Mater. 60 (2009) 211–213.
[29] X.P. Xiao, Z.Y. Yi, T.T. Chen, R.Q. Liu, H. Wang, Suppressing Spinodal decomposition by adding Co into Cu-Ni-Si alloy, J. Alloy. Compd. 660 (2015).
[30] Z. Rdzawski, J. Stobrawa, Thermomechanical processing of Cu–Ni–Si–Cr–Mg alloy, Mater. Sci. Technol. 9 (1993) 142–150.
[31] R. Monzen, C. Watanabe, Microstructure and mechanical properties of Cu–Ni–Si alloys, J. Soc. Mater. Sci. Jpn. 483–484 (2008) 117–119.
[32] C. Watanabe, S. Takeshita, R. Monzen, Effects of small addition of Ti on strength and microstructure of a Cu-Ni-Si alloy, Metall. Mater. Trans. A 46 (2015) 2469–2475.
[33] S.A. Lockyer, F.W. Noble, Fatigue of precipitate strengthened Cu–Ni–Si alloy, Mater. Sci. Technol. 15 (1999) 1147–1153.
[34] J.W. Martin, In Micromechanism in Particle-Hardened Alloys, In, Cambridge University Press, Cambridge 1984, p. 44.
[35] H.H. Fu, D.J. Benson, M.A. Meyers, Analytical and computational description of effect of grain size on yield stress of metals, Acta Mater. 49 (2001) 2567–2582.
[36] H.T. Zhou, J.W. Zhong, X. Zhou, Z.K. Zhao, Q.B. Li, Microstructure and properties of Cu–1.0Cr–0.2Zr–0.03Fe alloy, Mater. Sci. Eng.: A 498 (2008) 225–230.
[37] S. Tanaka, M. Mizusawa, H. Miura, T. Hagisawa, The influence of Zr, P additions on microstructure and ductility of Cu-Ni-Si forged alloys, J. Jpn. Inst. Met. 78 (2014) 7–15.
[38] E. Donoso, R. Espinoza, M. Dianez, J. Criado, Microcalorimetric study of the annealing hardening mechanism of a Cu–2.8Ni–1.4Si (at%) alloy, Mater. Sci. Eng. A-Struct. Mater. Prop. Microstruct. Process. 556 (2012) 612–616.